

Frequency-tunable microwave field detection in an atomic vapor cell

Andrew Horsley and Philipp Treutlein

Citation: *Appl. Phys. Lett.* **108**, 211102 (2016); doi: 10.1063/1.4950805

View online: <http://dx.doi.org/10.1063/1.4950805>

View Table of Contents: <http://aip.scitation.org/toc/apl/108/21>

Published by the [American Institute of Physics](http://www.aip.org)

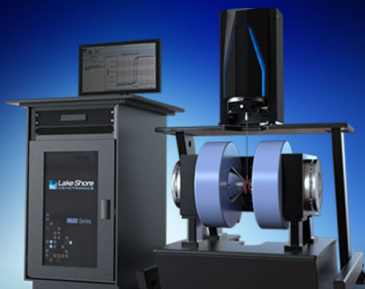
Articles you may be interested in

[Simple microwave field imaging technique using hot atomic vapor cells](#)

Appl. Phys. Lett. **101**, 181107181107 (2012); 10.1063/1.4760267




Lake Shore
CRYOTRONICS



NEW 8600 Series VSM

For fast, highly sensitive
measurement performance

LEARN MORE 

Frequency-tunable microwave field detection in an atomic vapor cell

Andrew Horsley^{a)} and Philipp Treutlein^{b)}
 Departement Physik, Universität Basel, CH-4056 Basel, Switzerland

(Received 26 February 2016; accepted 5 May 2016; published online 23 May 2016)

We use an atomic vapor cell as a frequency tunable microwave field detector operating at frequencies from GHz to tens of GHz. We detect microwave magnetic fields from 2.3 GHz to 26.4 GHz, and measure the amplitude of the σ_+ component of an 18 GHz microwave field. Our proof-of-principle demonstration represents a four orders of magnitude extension of the frequency tunable range of atomic magnetometers from their previous dc to several MHz range. When integrated with a high-resolution microwave imaging system [Horsley *et al.*, New J. Phys. **17**, 112002 (2015)], this will allow for the complete reconstruction of the vector components of a microwave magnetic field and the relative phase between them. Potential applications include near-field characterisation of microwave circuitry and devices, and medical microwave sensing and imaging. *Published by AIP Publishing.* [<http://dx.doi.org/10.1063/1.4950805>]

Atomic vapor cell magnetometers are among the most sensitive detectors for magnetic fields^{2–4} and show promise in applications including gyroscopes,⁵ explosives detection,⁶ materials characterization,^{7–9} in MRI for both medical¹⁰ and microfluidics applications,¹¹ and for magnetic imaging of the human heart^{12,13} and brain.^{14–17} Tunable atomic magnetometers have previously operated from dc to rf of a few MHz. In this letter, we demonstrate the principle of a continuously frequency tunable microwave magnetometer, capable of detecting magnetic fields from GHz to tens of GHz frequencies. This represents a four orders of magnitude extension of the atomic magnetometer frequency tunable range. Potential applications include near-field characterisation of microwave circuitry,^{1,18–20} and medical microwave sensing and imaging,^{21–23} where high resolution and intrinsically calibrated atomic sensors could replace bulky and field-perturbing antennas.

At the fixed microwave frequency of 6.8 GHz, we have previously used atoms to produce polarisation-resolved images of microwave magnetic near-field distributions.^{1,24–27} We have achieved $50 \times 50 \times 140 \mu\text{m}^3$ spatial resolution and $1 \mu\text{T}/\text{Hz}^{-1/2}$ sensitivity, observing good agreement between the measured fields and simulations for simple test structures.¹ (Atom-like) nitrogen vacancy (NV) centres have recently been used for nanoscale near-field detection²⁸ and imaging,²⁹ and microwave *electric* field imaging has also been demonstrated at discrete frequencies using Rydberg atoms.^{30–33} To-date, however, there has been no atomic sensor available for the detection of fields at arbitrary microwave frequencies, as required for most applications.

Our frequency-tunable sensing scheme is able to operate in either of two modes: to detect microwaves of unknown frequency (i.e., as a microwave spectrum analyzer); or to accurately measure the amplitudes of microwave magnetic fields (B_{mw}) of known frequency. In this letter, we focus on the latter, measuring B_{mw} through coherent

Rabi oscillations driven by the microwave on atomic hyperfine transitions.^{24,25} The atomic transitions are sensitive to a narrow microwave frequency band, and we use a dc magnetic field (B_{dc}) to tune the transition frequency to the desired value. This is conceptually similar to rf magnetometry, where a dc magnetic field is used to tune the Zeeman splitting of adjacent m_F states.³ However, much larger dc fields are required for microwave frequencies, bringing us into the hyperfine Paschen–Back regime. Moreover, since our technique is based on measurements of frequency rather than amplitude, it is intrinsically calibrated and less sensitive to environmental noise. In this letter, we work with the ⁸⁷Rb hyperfine ground states; however, our technique is applicable to any microwave magnetic dipole transition with optical read-out of one of the states, such as other alkali atoms and NV centres.

Figure 1 shows the splitting of the ⁸⁷Rb $5S_{1/2}$ ground state in an applied dc magnetic field, calculated using the Breit–Rabi formula.³⁴ We label the 8 hyperfine states $A_1 \rightarrow A_8$, in order of increasing energy. At $B_{\text{dc}} = 0$, the states are grouped according to the $|F, m_F\rangle$ basis defined by the atomic Hamiltonian, and split by 6.8 GHz. As B_{dc} is increased, the hyperfine states move towards the $|I, m_I, J, m_J\rangle$ basis defined by the dc field. This is accompanied by a corresponding shift in transition frequencies and coupling strengths between the hyperfine states. An applied microwave field will drive Rabi oscillations on a given transition that has been tuned to resonance. The amplitude of the microwave vector component B_γ is given by the measured Rabi oscillation frequency, Ω_R , the transition matrix element, and well-known fundamental constants. For a microwave resonant with transition T_{if} , we have

$$B_\gamma = |\alpha_{if}| \frac{\hbar}{\mu_B} |\Omega_R|, \quad (1)$$

where $\gamma = -, \pi, +$ is the polarisation of the transition, and

$$\alpha_{if} \equiv \frac{1}{2\langle A_f | J_y | A_i \rangle}. \quad (2)$$

^{a)}andrew.horsley@unibas.ch

^{b)}philipp.treutlein@unibas.ch

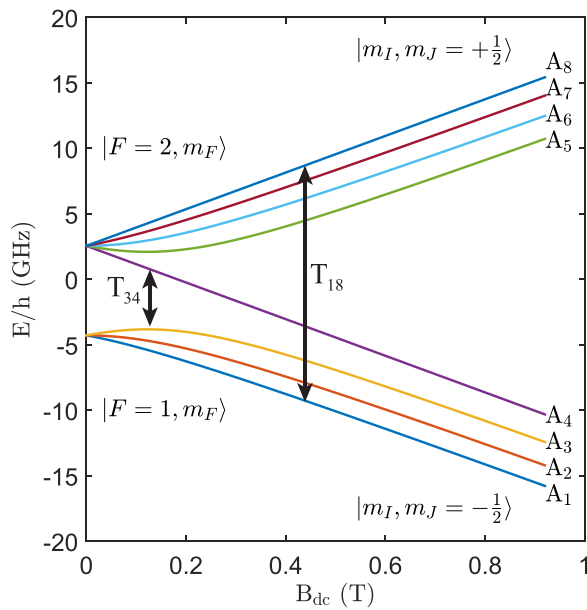


FIG. 1. Energy splitting of the ^{87}Rb hyperfine ground state levels as a function of applied dc magnetic field. Arrows indicate the hyperfine transitions used in this work.

The coupling factor α_{ij} is a function of the applied dc magnetic field. As B_{dc} increases, $\alpha \rightarrow 1$ for the σ_+ polarised transitions, and $\alpha \rightarrow 0$ for the σ_- and π transitions. For ^{87}Rb , we can find σ_- (π) transitions where $|\alpha| > 0.15$ for microwave frequencies within the range 2.2 – 9.1 GHz (5.9 – 22.8 GHz).³⁵ Strong σ_+ transitions are available for all frequencies. Previous B_{mw} reconstruction schemes have relied on the presence of strong π transitions.¹ However, it is possible to completely reconstruct the vector components of the microwave magnetic field amplitude, and the relative phases between them, using only σ_+ transitions.³⁵ The reconstruction then requires measurements

of B_+ with the dc magnetic field both parallel and anti-parallel to each of the lab-frame x , y , and z axes. In this letter, we address two microwave transitions: the σ_+ polarised T_{18} transition and the σ_- polarised T_{34} transition.

We use a 2 mm thick, microfabricated vapor cell (Fig. 2(a)), filled with natural Rb and 63 mbar of N_2 buffer gas.^{26,36} Doppler and collisional broadening result in an optical linewidth of 1.5 GHz. We use a 780 nm laser, linearly polarised along B_{dc} , for both optical pumping and probing. A water-cooled solenoid³⁷ provides dc magnetic fields up to 0.8 T (Fig. 2(b)). We heat the vapor cell using a 2 W laser at 1500 nm^{35,38} and obtain the cell temperature by fitting optical absorption spectra (taken at $B_{\text{dc}}=0$) with the model described in Ref. 39.

We can detect microwaves over a broad range of frequencies. Figure 3(a) shows experimentally obtained double-resonance (DR) peaks for microwaves spanning frequencies from 2.3 GHz to 26.4 GHz. The laser beam is applied continuously, and its frequency is tuned to resonance with one of the hyperfine states. This partially depopulates the state through optical pumping. Through the transmission of the laser onto a photodiode, we monitor the change in optical density (OD_{mw}) as we sweep the frequency of an applied microwave field. Whenever the microwave frequency crosses a hyperfine transition coupling to the optically pumped state, we see a peak in OD_{mw} , corresponding to repopulation of the state. Each peak in Fig. 3 represents a separate measurement, with B_{dc} changed between measurements. Peaks in the range 7 – 26.4 GHz (red) were measured on the σ_+ T_{18} transition, while peaks in the range 2.3 – 6 GHz (blue) were measured on the σ_- T_{34} transition. The laser beam probed the approximate spatial centre of the dc magnetic field (see Fig. 4(b)), with inhomogeneities in the dc field resulting in a 1 MHz (FWHM) DR linewidth. The peak area is proportional to Ω_R ; however, it is also

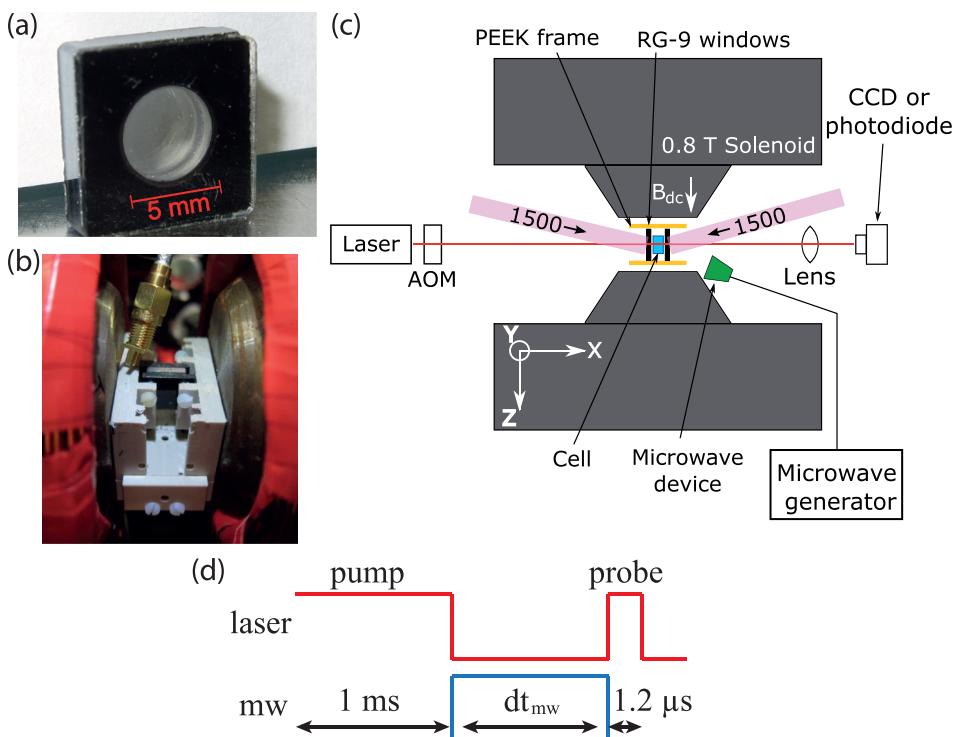


FIG. 2. (a) Vapor cell; (b) the experiment setup, showing the vapor cell sandwiched between two RG-9 glass pieces and mounted on the PEEK frame inside the solenoid. The gold microwave output coupler can be seen above the cell; (c) schematic of the experiment setup; (d) the Rabi sequence used to obtain microwave amplitudes.

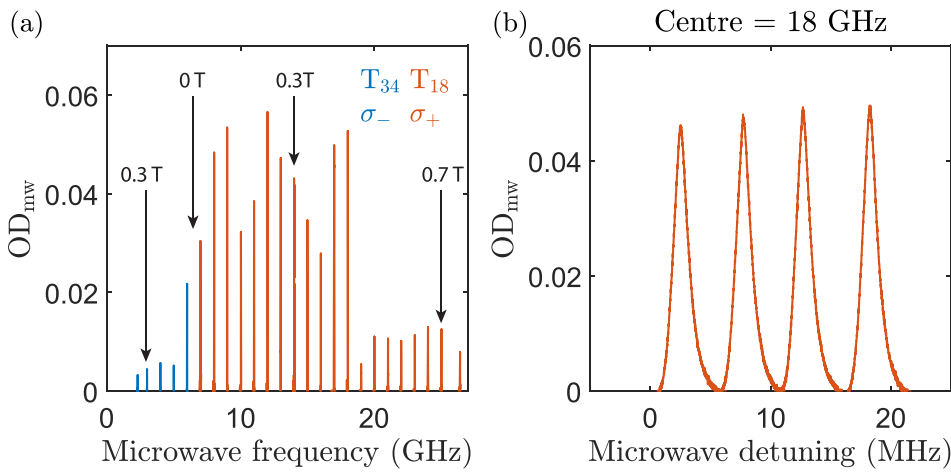


FIG. 3. Detection of microwave signals at arbitrary frequencies. (a) DR detection of frequencies ranging from 2.3 GHz to 26.4 GHz. Each peak corresponds to a single experimental run taken using a different B_{dc} . The data were taken on both the T_{34} (blue) and T_{18} (red) transitions, and show the change in optical density induced by the microwave. Labels in black indicate relevant B_{dc} strengths. (b) DR peaks for frequencies near 18 GHz, showing fine-tuning of the detection frequency by adjusting B_{dc} .

sensitive to fluctuations in the laser intensity and cell temperature, and calibration with a known field is required to extract Ω_R . For fixed conditions (not shown), we observe the expected linear scaling of the peak area with the square-root of the microwave power. The lower limit on microwave frequency in Fig. 3(a) was imposed by the asymptotic behaviour of the T_{34} transition frequency at high B_{dc} .³⁵ Other transitions (e.g., T_{45}) are available with frequencies down to dc, in which case the lower detection limit will be given by the optical distinguishability of the neighbouring hyperfine states, in general on the order of the 0.5 GHz Doppler broadening in a cell without buffer gas. The upper frequency limit is given only by technical limitations, e.g., the available B_{dc} strength, or in our case, the microwave frequency generator.

The dc magnetic field provides fine control over the microwave detection frequency, as shown in Fig. 3(b). Each DR peak represents a single measurement on the T_{18} transition, with the zero of the horizontal axis corresponding to a microwave frequency of 18 GHz. By scanning B_{dc} , such DR measurements could be used in a spectrum analyser mode, to search for microwave fields of unknown frequency.

For an accurate measure of the B_{mw} amplitude, we need to measure the Rabi frequency directly. We demonstrate this by measuring the σ_+ amplitude of an 18 GHz microwave. The observed oscillations are a function of both microwave amplitude ($\propto \Omega_R$) and detuning from resonance (Δ), with a frequency $\Omega = \sqrt{\Omega_R^2 + \Delta^2}$. In general, it is simple to directly

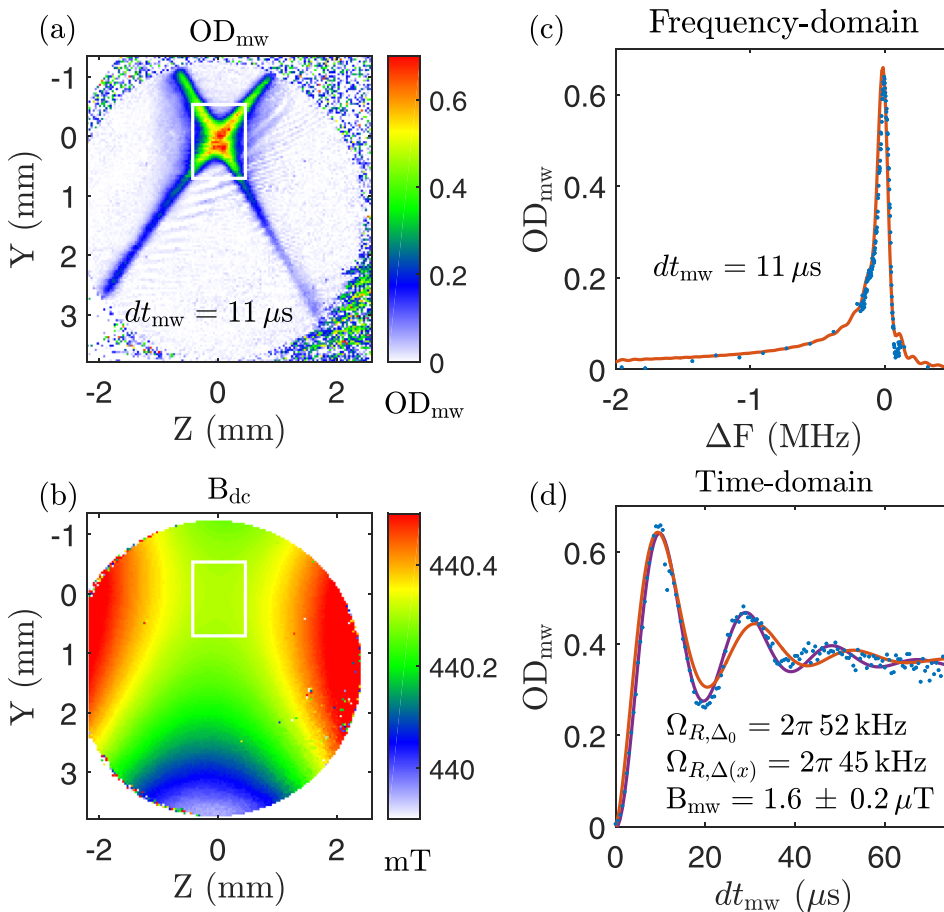


FIG. 4. Measuring an 18.003 GHz microwave field amplitude. Experimentally obtained images of (a) OD_{mw} for a microwave pulse resonant with the T_{18} transition in the B_{dc} field centre; (b) map of the local B_{dc} field extracted from measurements as in (a). The circular field of view is given by the cell walls, and the white boxes indicate the region appropriate for microwave sensing; (c) and (d) scans in the frequency and time domains, for the pixel at ($z=0$ mm, $y=0$ mm). Fits are shown assuming a constant microwave detuning along the x -axis (purple, time domain only, Ω_{R,Δ_0}), and allowing for an inhomogeneous fit to time and frequency domain data, $\Omega_{R,\Delta(x)}$.

measure the detuning, e.g., from the peak of a DR scan. We use a relatively thick cell in our proof-of-principle setup, however, and must account for a non-negligible B_{dc} inhomogeneity along the x -axis, which the laser integrates over as it passes through the cell. Our experiment “Rabi” sequence, shown schematically in Fig. 2(d), begins with an optical pumping pulse to depopulate the A_1 state. A microwave pulse of duration dt_{mw} then drives Rabi oscillations between the A_1 and A_8 states, and we detect the repopulation of the A_1 state (i.e., OD_{mw}) with a $1.2 \mu s$ probe laser pulse. We repeat this sequence, scanning either the frequency (Fig. 4(c)) or duration (Fig. 4(d)) of the microwave pulse. The frequency domain scan primarily constrains B_{dc} (Fig. 4(b)), and we extract the B_{mw} amplitude by simultaneously fitting the two scans.³⁵ In future setups, the frequency domain scan will be unnecessary.

We used the T_{18} transition for sensing, with the frequency of the laser tuned to address the A_1 level. A solenoid field of $B_{dc} \approx 0.44$ T tuned the T_{18} transition of atoms in the B_{dc} field centre to resonance with the applied 18 GHz microwave. At this dc field, the A_1 level is optically well-resolved,⁴⁰ and almost all of the measured optical density of $OD = 2.1$ was due to atoms in the A_1 state. The frequency domain scan was performed around 18.003 GHz with a fixed microwave pulse duration of $dt_{mw} = 11 \mu s$, corresponding roughly to a π pulse in the centre of the B_{dc} field, while the time domain scan was performed with a fixed frequency of 18.003 GHz.

We are working towards frequency tunable microwave imaging, and therefore use a CCD camera and the technique of absorption imaging for detection.^{1,40,41} The laser illuminates the entire cell, and we obtain images of OD_{mw} (Fig. 4(a)). Due to inhomogeneities in the B_{dc} field, we only present microwave detection for a single pixel near the B_{dc} centre. If only single-channel sensing is required, real-time monitoring of the Rabi oscillations should also be possible using a photodiode and an off-resonant probe laser. The atomic response traced a contour line of the B_{dc} field in the cell, as shown in Fig. 4(a), which shows an image of OD_{mw} for an $11 \mu s$ long 18.003 GHz microwave pulse. Scanning the microwave frequency (Fig. 4(c)), we could quickly estimate the local T_{18} transition frequency from the peak in OD_{mw} . Using the Breit–Rabi formula, this transition frequency yielded an image of the applied B_{dc} , shown in Fig. 4(b). We see that the solenoid field is saddle-shaped, homogeneous to better than 10^{-3} , but nonetheless varying by several Gauss over the cell. The plane of the image is slightly offset from the $x = 0$ centre of the solenoid field.

The simultaneous fit of the Figs. 4(c) and 4(d) frequency and time domain data, described in detail in the supplementary material, yielded a Rabi frequency of $\Omega_{R,\Delta(x)} = 2\pi 45$ kHz, corresponding to $B_{mw} = 1.6 \mu T$. The shape of the frequency scan data in Fig. 4(c) is primarily determined by the variation in B_{dc} along the x -axis, and is well-matched by the fit. The peak corresponds to atoms around the B_{dc} centre, where the field is relatively flat, while the long tail is due to the drop-off of B_{dc} away from the centre. The time domain fit in Fig. 4(d) underestimates the oscillation frequency, due to constraints imposed by the simultaneous fitting of time and frequency domain data with our relatively simple model. In fact, we find much better agreement with the time domain

data if we simply assume a constant $\Delta_0 = -4$ kHz, given by the frequency domain peak position, and fit to the time domain data only. This is shown by the purple line in Fig. 4(d), and we obtain $\Omega_{R,\Delta_0} = 2\pi 52$ kHz, corresponding to $B_{mw} = 1.8 \mu T$. By neglecting the range of larger detunings along the x -axis, this value serves as an upper bound on B_{mw} . We can therefore estimate a B_{mw} accuracy of 10% in our current proof-of-principle setup. We emphasise that in a high resolution setup using a thinner vapor cell,¹ the image analysis will be much simpler, with B_{mw} directly extracted from time domain data and accuracy on the 10^{-3} level.

In conclusion, we have presented a proof-of-principle demonstration of microwave magnetic field detection for microwaves of any frequency, obtaining the amplitude of the σ_+ component of an 18 GHz microwave field, and detecting magnetic fields at frequencies from 2.3 GHz to 26.4 GHz. Magnetic field detection of frequencies up to 50 GHz should be achievable with room-temperature iron-bore solenoids (which can operate to ~ 1.6 T), and given sufficient dc field homogeneity, it may be possible to detect fields up to 1 THz using the strongest available superconducting solenoids (> 35 T). It would be interesting to explore the frequency tunability presented here with other detection techniques, such as Faraday rotation or EIT, and with other systems, such as NV centres.²⁹

Our frequency tunable detection provides an essential step towards an atom-based characterisation tool for microwave devices operating at any frequency. To realise this in practical form, the frequency tunability demonstrated in this letter should now be integrated with a high resolution imaging setup.¹ We note, however, that for some devices, such as circulators, the large applied B_{dc} fields may significantly perturb the device operation. High spatial resolution, provided by a thin vapor cell, will have the added benefit of significantly reducing our sensitivity to B_{dc} inhomogeneities. For a $200 \mu m$ thick cell operating in the B_{dc} field shown in Fig. 4(b), B_{dc} variation along the x -axis should be negligible, on the order of $2\pi \times 1$ kHz. The transverse variation over a $50 \times 50 \mu m^2$ pixel at the B_{dc} centre would be $2\pi \times 0.2$ kHz, increasing to $2\pi \times 80$ kHz at a distance 1 mm either side of the centre. This is entirely acceptable compared to the tens to hundreds of kHz Rabi frequencies observed in Ref. 1. Moreover, the B_{dc} inhomogeneity could also be reduced by using shimming coils. We expect the sensitivity to be slightly better than for the fixed-frequency imaging reported in Ref. 1, due to the suppression of Rb spin-exchange relaxation in large B_{dc} fields.⁴² The integrated setup could be miniaturised by replacing the bulky solenoid with permanent rare-earth magnets, with B_{dc} adjusted through the magnet separation.^{43,44}

This work was supported by the Swiss National Science Foundation (SNFS). We thank G. Mileti, C. Affolderbach, and Y. Pétremand for providing the vapor cell, and the group of P. Maletinsky for the loan of microwave circuitry. We also thank M. Belloni for interesting discussions, and C. Affolderbach for careful reading of the manuscript.

¹A. Horsley, G.-X. Du, and P. Treutlein, *New J. Phys.* **17**, 112002 (2015).

²D. Budker and M. Romalis, *Nat. Phys.* **3**, 227 (2007).

- ³I. M. Savukov, S. J. Seltzer, M. V. Romalis, and K. L. Sauer, *Phys. Rev. Lett.* **95**, 063004 (2005).
- ⁴D. Sheng, S. Li, N. Dural, and M. V. Romalis, *Phys. Rev. Lett.* **110**, 160802 (2013).
- ⁵E. A. Donley, J. L. Long, T. C. Liebisch, E. R. Hodby, T. A. Fisher, and J. Kitching, *Phys. Rev. A* **79**, 013420 (2009).
- ⁶S.-K. Lee, K. L. Sauer, S. J. Seltzer, O. Alem, and M. V. Romalis, *Appl. Phys. Lett.* **89**, 214106 (2006).
- ⁷M. V. Romalis and H. B. Dang, *Mater. Today* **14**, 258 (2011).
- ⁸C. Deans, L. Marmugi, S. Hussain, and F. Renzoni, *Appl. Phys. Lett.* **108**, 103503 (2016).
- ⁹A. Wickenbrock, N. Leefer, J. W. Blanchard, and D. Budker, *Appl. Phys. Lett.* **108**, 183507 (2016).
- ¹⁰I. Savukov and T. Karaulanov, *J. Mag. Res.* **231**, 39 (2013).
- ¹¹S. Xu, C. W. Crawford, S. Rochester, V. Yashchuk, D. Budker, and A. Pines, *Phys. Rev. A* **78**, 013404 (2008).
- ¹²G. Bison, N. Castagna, A. Hofer, P. Knowles, J.-L. Schenker, M. Kasprzak, H. Saudan, and A. Weis, *Appl. Phys. Lett.* **95**, 173701 (2009).
- ¹³O. Alem, T. H. Sander, R. Mhaskar, J. LeBlanc, H. Eswaran, U. Steinhoff, Y. Okada, J. Kitching, L. Trahms, and S. Knappe, *Phys. Med. Biol.* **60**, 4797 (2015).
- ¹⁴I. Savukov and T. Karaulanov, *Appl. Phys. Lett.* **103**, 43703 (2013).
- ¹⁵C. N. Johnson, P. D. D. Schwindt, and M. Weisend, *Phys. Med. Biol.* **58**, 6065 (2013).
- ¹⁶R. Wyllie, M. Kauer, R. T. Wakai, and T. G. Walker, *Opt. Lett.* **37**, 2247 (2012).
- ¹⁷V. K. Shah and R. T. Wakai, *Phys. Med. Biol.* **58**, 8153 (2013).
- ¹⁸S. Sayil, D. J. Kerns, and S. Kerns, *IEEE Trans. Instrum. Meas.* **54**, 2082 (2005).
- ¹⁹T. Dubois, S. Jarrix, A. Penarier, P. Nouvel, D. Gasquet, L. Chusseau, and B. Azais, *IEEE Trans. Instrum. Meas.* **57**, 2398 (2008).
- ²⁰G. M. Sardi, A. Lucibello, M. Kasper, G. Gramse, E. Proietti, F. Kienberger, and R. Marcelli, *Appl. Phys. Lett.* **107**, 033107 (2015).
- ²¹E. C. Fear, S. C. Hagness, P. M. Meaney, M. Okoniewski, and M. A. Stuchly, *IEEE Microwave Mag.* **3**, 48 (2002).
- ²²N. Nikolova, *IEEE Microwave Mag.* **12**, 78 (2011).
- ²³R. Chandra, H. Zhou, I. Balasingham, and R. M. Narayanan, *IEEE Trans. Biomed. Eng.* **62**, 1667 (2015).
- ²⁴P. Böhi, M. F. Riedel, T. W. Hänsch, and P. Treutlein, *Appl. Phys. Lett.* **97**, 051101 (2010).
- ²⁵P. Böhi and P. Treutlein, *Appl. Phys. Lett.* **101**, 181107 (2012).
- ²⁶A. Horsley, G.-X. Du, M. Pellaton, C. Affolderbach, G. Mileti, and P. Treutlein, *Phys. Rev. A* **88**, 063407 (2013).
- ²⁷C. Affolderbach, G.-X. Du, T. Bandi, A. Horsley, P. Treutlein, and G. Mileti, *IEEE Trans. Instrum. Meas.* **64**, 3629 (2015).
- ²⁸P. Wang, Z. Yuan, P. Huang, X. Rong, M. Wang, X. Xu, C. Duan, C. Ju, F. Shi, and J. Du, *Nat. Commun.* **6**, 6631 (2015).
- ²⁹P. Appel, M. Ganzhorn, E. Neu, and P. Maletinsky, *New J. Phys.* **17**, 112001 (2015).
- ³⁰J. A. Sedlacek, A. Schwettmann, H. Kübler, R. Löw, T. Pfau, and J. P. Shaffer, *Nat. Phys.* **8**, 819 (2012).
- ³¹C. Holloway and J. Gordon, *Appl. Phys. Lett.* **104**, 244102 (2014).
- ³²H. Q. Fan, S. Kumar, R. Daschner, H. Kübler, and J. P. Shaffer, *Opt. Lett.* **39**, 3030 (2014).
- ³³H. Fan, S. Kumar, J. Sedlacek, H. Kübler, S. Karimkashi, and J. P. Shaffer, *J. Phys. B* **48**, 202001 (2015).
- ³⁴D. A. Steck, see <http://steck.us/alkalidata> for Rubidium 87 D Line Data (version 2.1.4, last revised 23 December 2010).
- ³⁵See supplementary material at <http://dx.doi.org/10.1063/1.4950805> for further details on the experiment and data analysis, as well as discussions of hyperfine transitions in arbitrary external dc magnetic fields, and the reconstruction of microwaves of arbitrary frequency.
- ³⁶M. Pellaton, C. Affolderbach, Y. Pétremand, N. de Rooij, and G. Mileti, *Phys. Scr.* **T149**, 014013 (2012).
- ³⁷Brücker, B-E 10 solenoid with B-MN C4 power supply, built in 1974.
- ³⁸R. Mhaskar, S. Knappe, and J. Kitching, *Appl. Phys. Lett.* **101**, 241105 (2012).
- ³⁹M. A. Zentile, J. Keaveney, L. Weller, D. J. Whiting, C. S. Adams, and I. G. Hughes, *Comput. Phys. Commun.* **189**, 162 (2015).
- ⁴⁰A. Horsley, Ph.D. thesis (Department of Physics, University of Basel, Switzerland, 2015).
- ⁴¹A. Horsley, G.-X. Du, M. Pellaton, C. Affolderbach, G. Mileti, and P. Treutlein, in *Proceedings of the 2013 Joint IEEE-UFFC, EFTF and PFM Symposium* (2013), p. 575.
- ⁴²S. Kadlecsek, T. Walker, D. K. Walter, C. Erickson, and W. Happer, *Phys. Rev. A* **63**, 052717 (2001).
- ⁴³L. Weller, K. S. Kleinbach, M. A. Zentile, S. Knappe, I. G. Hughes, and C. S. Adams, *Opt. Lett.* **37**, 3405 (2012).
- ⁴⁴M. A. Zentile, R. Andrews, L. Weller, S. Knappe, C. S. Adams, and I. G. Hughes, *J. Phys. B* **47**, 075005 (2014).